J Mater Sci (2012) 47:702–710
DOI 10.1007/s10853-011-5843-7

Interactions at fiber/matrix interface in short fiber reinforced amorphous thermoplastic composites modified with micro- and nano-fillers

Nihat Ali Isitman · Muratahan Aykol · Cevdet Kaynak

Received: 13 June 2011 / Accepted: 2 August 2011 / Published online: 16 August 2011

Abstract This study aims at systematically extracting fiber/matrix interfacial strength in short-glass fiber-reinforced polymer composites using an experimental micromechanics approach which employs mechanical properties and residual fiber length distributions to derive the apparent interfacial shear strength. We started from neat high-impact polystyrene matrix short-glass fiber-reinforced composites (HIPS/GF) with varying fiber loading and proceeded toward HIPS/GF hybrid composites containing micro- and nano-fillers where complex fiber/matrix interfacial interactions exist. It was found that apparent interfacial shear strength does not vary with fiber content, while the presence of fillers with different length-scales alters fiber/matrix interactions depending on their influence on physical properties of the polymer matrix, particularly in the vicinity of reinforcing fiber surfaces.

Introduction

The resistance of the interface between fiber reinforcement and polymer matrix to shear determines the extent of stress transferred to fibers and hence the reinforcement efficiency of utilized fibers. While the strength of the interface can be evaluated by experimental micromechanics such as fragmentation or pull-out tests, the in situ response of the fiber/matrix interface to shear may highly deviate from that isolated interfacial failure. Despite the fundamental basis of experimental micromechanics, in practice, obtaining consistent results was shown to be difficult using direct interface measurements due to stress concentrations where resultant stress measurements were argued to provide interface properties with no physical meaning [1–7]. Besides, actual composites contain a great many side effects such as order of radial and axial stresses on fibers, alterations in the physical properties of matrix globally or in the vicinity of interface, location at which actual shear takes place and fiber surface roughness, to name a few important ones. Estimation of the apparent interfacial shear strength (IFSS), as a composite property, overcomes this complexity and reveals the overall contribution originating from each effect. In this respect, Thomason [8–11] has recently utilized a modified Bader–Bowyer approach to investigate IFSS in various kinds of fiber-reinforced composites under different conditions. A similar variant of the theory, which continuously handles the stress–strain response, is the continuum micromechanics model of short fiber-reinforced thermoplastics [12]. It provides an efficient link between mechanical properties and apparent IFSS. In some previous cases [13–15], the versatility of the approach practically allowed the prediction of physically meaningful IFSS.

In recent studies by Thomason [16–18], it was found that IFSS diminishes rapidly with increasing fiber content in crystallizable-matrix composites involving sized fibers, while IFSS was slightly lowered with unsized fiber content. It can be stated that higher fiber contents create higher cooling rates, which in turn result in lower degree of polymer crystallinity. It is thought that if one can experimentally avoid the residual stresses at the interfacial zone due to crystallization shrinkage, IFSS can be traced under somewhat more idealized conditions. Therefore, we first conducted an investigation on the effect of fiber content on IFSS using an amorphous thermoplastic matrix.

N. A. Isitman · M. Aykol · C. Kaynak (✉)
Department of Metallurgical and Materials Engineering, Middle East Technical University, 06531 Ankara, TR, Turkey
e-mail: ckaynak@metu.edu.tr

Besides, short fiber-reinforced thermoplastics are often modified with micro-fillers (MF), the main concern being extension of material properties or cost-oriented. For instance, fillers providing substantial improvements in flame retardancy of short-fiber composites are widely employed to broaden the field of applications [13, 19–21]. These fillers almost always increase the elastic modulus of the composite but tensile strength, toughness, and ductility may become significantly deteriorated. Further modification of short-fiber composites can be achieved using nano-fillers (NF) such as layered silicates. These newly emerging composite materials exploit synergistic reinforcement at different length scales, i.e., microscopic fiber-reinforcement combined with exfoliated nanoscopic layered silicates [22]. In addition to the scarcity of literature concerning these hybrid thermoplastic composites, there exists only a single study dealing with the influence of nano-filler on the fiber/matrix interface [23]. Therefore, this study will place particular emphasis on the investigation of a fundamental property that governs mechanical properties, i.e., the apparent IFSS in short-fiber reinforced thermoplastics, particularly in the presence of fillers with different length scales. Since any dispersed second phase in the matrix, whether its dimensions are in the micro- or nano-scale, has a different potential to alter the physical properties of polymer matrix upon processing, the deliberate choice of the amorphous matrix allowed at least the exclusion of dissimilar degrees of crystallization and its incomparable influences on IFSS.

Experimental

Polymer matrix used was an extrusion grade high-impact polystyrene (HIPS; Dow Styron A-tech 1175). Chopped glass fibers (GF) treated with γ-aminopropyltrimethoxysilane (Camelyaf, PA1) had 13 μm nominal diameter and 4.5 mm initial length. Micro-filler used was aluminum trihydroxide (Nabaltec Apyral-16) with an average particle size of 12 μm. Nano-filler used was an organically modified montmorillonite clay mineral (Cloisite 10A) obtained from Southern Clay Products, Inc. All the studied formulations listed in Table 1 were produced by melt compounding using a micro-compounder (DSM Xplore 15 ml Micro-Compounder) at a constant barrel temperature setting of 210 °C with 3 min mixing time. The equipment is capable of repeated mixing of the same input material via a backflow channel within the barrel which makes it comparable to a normal size extruder.

Specimens for testing and characterization were produced by ram-type lab-scale injection molding devices (Daca Instruments Microinjector and DSM Xplore 12 mL Injection Molding Machine) at barrel and mold temperatures of 210 and 55 °C, respectively.

Table 1 Compositions (wt%) and designations of studied materials

Designation	Glass fiber (GF)	Micro-filler (MF)	Nano-filler (NF)
HIPS	–	–	–
HIPS/MF	–	15	–
HIPS/NF	–	–	3
HIPS/MF/NF	–	15	3
HIPS/GF	10–20–30–40–50	–	–
+MF	20	15	–
+NF	20	–	3
+MF/NF	20	15	3

Fiber length distributions (FLD) were determined by burning off the polymer matrix at elevated temperatures and using semi-automated photomicrography to analyze ~600 fibers for each specimen. Tension tests were carried out on dog-bone shaped samples with 2-mm thickness, 7.4-mm width, and gauge length of 80 mm using a Shimadzu AGS-J (10 kN) universal testing machine at a crosshead speed of 1 mm/min. Dynamic mechanical analysis (DMA) was performed on samples with $4 \times 10 \times 80$ mm^3 dimensions using single cantilever bending mode on a Perkin Elmer Pyris Diamond DMA. X-ray diffraction (XRD) was performed on a Rigaku D-Max 2200 with CuKα radiation. Scanning electron microscopy (SEM) was carried out using a JEOL JSM-6400 SEM on gold sputtered fracture surfaces of tension test specimens. Ultra-thin sections were obtained using an ultramicrotome (Leica EM UC 6). Transmission electron microscopy (TEM) was conducted with a high resolution microscope (JEOL JEM-2100, LaB_6) under 200 kV acceleration voltage.

Results and discussion

Strength of a short-fiber reinforced composite can be simply modeled by the modified rule of mixtures incorporating FLD and fiber orientation distribution (FOD) efficiency factors (η_{FLD} and η_{FOD}) as,

$$\sigma_c = \eta_{FOD}\eta_{FLD}\sigma_f V_f + \sigma_m V_m \quad (1)$$

where σ and V denote stress and volume fraction, and subscripts c, f, and m denote composite, fiber, and matrix, respectively. A micromechanical approach was recently developed [12] which incorporates the IFSS embedded FLD efficiency parameter which reads

$$\eta_{FLD}(\varepsilon, K) = \frac{1}{2}\left[e^{-K\ell_c^n} - \frac{\Gamma\left(\frac{1}{n}, K\ell_c^n\right) - \Gamma\left(\frac{1}{n}\right)}{\ell_c n\sqrt[n]{K}} - \ell_c\sqrt[n]{K}\Gamma\left(1 - \frac{1}{n}, K\ell_c^n\right)\right] \quad (2)$$

In brief, using tension test data for fiber free matrix and corresponding fiber reinforced composite, the value of η_{FLD}

at composite break (or yield) can be calculated by inserting composite and matrix elastic moduli (E_c and E_m), stresses at composite break or yield (σ_c^b and σ_m^b), composite strain at break or yield (ε_b) and fiber volume fraction (V_f) into

$$\eta_{FLD}^{b} = \left[\sigma_c^b - \sigma_m^b(1 - V_f)\right] / \left[(E_c - E_m(1 - V_f))\varepsilon_b\right] \quad (3)$$

In extrusion compounding, chopped glass fibers being fed into the barrel cannot retain their initial lengths and are continuously broken into a distribution of lengths as a consequence of fiber surface attrition through fiber–fiber, fiber–filler, and fiber–machine interactions [24–26]. Residual fiber lengths generally yield a statistical distribution according to their volume fractions, integration of which yields cumulative fiber volume fraction in the form $F(\ell, V_f) = 1 - e^{(-K.\ell^n)}$ where K and n denote the scale and shape parameters of distribution, respectively. The cumulative FLD is a more convenient form for handling numerical photomicrography data and transforming the discrete distribution to a continuous function. This transformation is quantified by the parameter K, which can be determined by a Least-squares fitting to the experimentally determined discrete FLD. Shapes of cumulative FLD curves were found to be best represented when a shape parameter of 2.5 is used for n [27]. Consequently, K becomes the only parameter reflecting the residual fiber length distribution upon extrusion compounding.

Then, by experimental determination of residual FLD for the composite, Eq. 2 can be iteratively solved to extract ℓ_c and consequently τ (IFSS) by the relation $\ell_c = E_f \varepsilon d (2\tau)^{-1}$. For simplicity, a graphical interpretation method was implemented [12] to evaluate IFSS from a combination of tension tests and residual FLDs as shown in Fig. 1.

Using the developed approach, the apparent fiber/matrix IFSS was successfully revealed in a wide range of short-fiber reinforced composite systems [13–15]. Figure 1 is a compilation (including data from this particular work) of graphically interpreted critical fiber lengths. Since the derived IFSS is an apparent composite property, any chemical or physical modification of the interfacial zone can be readily followed, even for complex systems. Assumptions of the model are essentially the same with that of Bader and Bowyer [28, 29], except for the assumption that fiber length distribution can be represented by a specific statistical distribution [30–33]. It is worth to note that all arguments related to the "break" of the composite are limited to yield which occurs in particular by crazing in HIPS matrix.

In order to obtain accurate results by the micromechanical approach for complex systems involving fillers in addition to the fiber reinforcement, the term "matrix" should be redefined incorporate all constituents (polymer, filler, etc.) making up the composite except for the reinforcing fibers. Consequently, as done in this study,

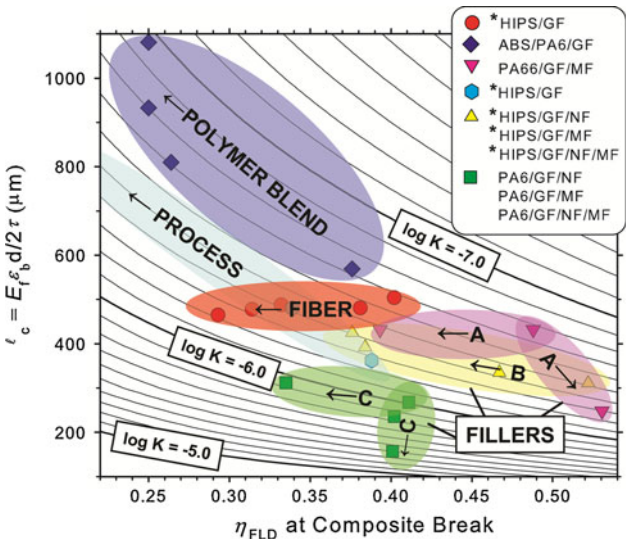

Fig. 1 Graphical interpretation of interfacial strength in a variety of short fiber composite systems revealing the influence of processing conditions, fiber content, polymer blend matrix composition, and the presence of fillers with different length-scales. Data from this study is denoted by an *asterisk*

properties of this fiber free "matrix" should be experimentally determined incorporating the effects of micro- and nano-scale fillers (except reinforcing fibers) on properties of the matrix polymer. For instance, determination of IFSS in a short-glass fiber-reinforced polymer containing both micro- and nano-scale fillers requires experimental determination of mechanical properties of the fiber free matrix, i.e., polymer containing the micro- and nano-scale fillers processed under the same conditions.

In this study, we chose this particular HIPS/GF system since HIPS does not show considerable enthalpic interactions with the utilized glass fibers and no stereoregularity meaning it is non-crystallizable. Therefore, a major component of IFSS can be related to the radial compressive residual stresses developing from the thermal expansion mismatch of the host polymer matrix and glass fiber during post-processing.

Figure 2a shows cumulative FLD of HIPS/GF composites with varying glass fiber content. Distributions were shifted progressively to shorter lengths with larger volume fraction of reinforcing fibers arising from the increased probability of attrition contacts during extrusion processing. The variation of the scale parameter K with fiber content was essentially linear, as shown in the inset of Fig. 2a. Besides, extrusion conditions and accompanying degradation in fiber lengths were also well-represented with K as plotted in Fig. 2b for varying extruder screw speed. These simple facts allow property interpolations to reduce the effort for material optimization, when combined with the micromechanical approach utilized here.

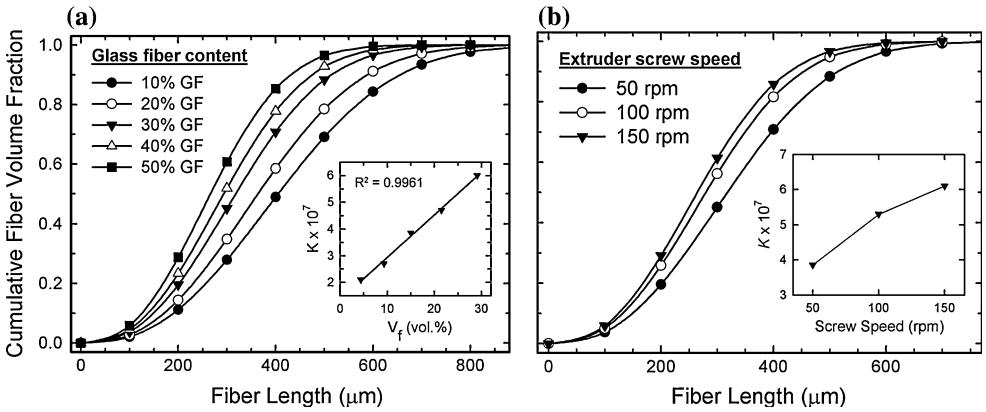

Fig. 2 Variation of FLD in HIPS/GF composites with **a** fiber content and **b** screw speed in extrusion. *Insets* show corresponding variations of FLD scale parameter K

Figure 3a shows that IFSS values determined for HIPS/GF system are independent of fiber content and reflect the shear yield strength of HIPS, the reason for which is that matrix morphology, interface chemistry, and the thermal contraction of chains in the close vicinity of fiber surfaces are not considerably affected by increasing fiber loading. As it can be depicted from the DMA curve of neat HIPS given in Fig. 4, HIPS is a glassy polymer and it possesses two glass transitions, higher temperature one being around 115.4 °C and lower temperature one being considerably below zero, at around −78.7 °C. It contains dispersed second phase rubber particles, and this rubber phase induces significant reduction in rigidity below the glass transition for polystyrene, which allows for the relaxation of axial or radial residual stresses on fibers during cooling regardless of fiber content. Critically observing the interfacial regions in micrographs of HIPS/GF composites given in Fig. 5, it can be concluded that composites with different fiber loadings had a similar feature, i.e., fibers being surrounded by dark rings, which indicates interfacial debonding by local deformation of matrix near fibers [34–36]. Regarding the processing conditions examined at $V_f = 0.15$ in Fig. 3b, an optimum in respect of IFSS and tensile strength was found which insures good wetting and provides homogenous dispersion. There appears to be a compromise between fiber-breakage (increase in K) and extent of good wetting/mixing as the extrusion screw speed is increased, revealing the optimum observed in IFSS.

The experimentally evidenced loss in strengthening rate (non-linear increase in composite strength) with increasing fiber content in HIPS/GF system (Fig. 3a) is mainly related to load transfer efficiency and can be modeled with the employed micromechanical approach which bears two efficiency parameters accounting for fiber length and orientation effects.The latter can be defined as [37];

$$\eta_{FOD} = [E_c - E_m(1 - V_f)]/E_f V_f \quad (4)$$

where elastic moduli are measured as $\varepsilon \to 0$; thus as $\eta_{FLD} \to 1$. This relation implies that if composite modulus E_c includes $E_m(1-V_f)$ with a modified rule of mixtures type linear dependence on V_f, matrix contributions in Eq. 4 will cancel each other and η_{FOD} will turn out independent of V_f. This is experimentally verified in Fig. 3a with the linear dependence of E_c on V_f, corresponding η_{FOD} values being in a narrow range of 0.21–0.24 for all different fiber contents.

On the other hand, η_{FLD} depends strictly on fiber lengths. Hence, the nonlinearity of fiber strengthening in Fig. 3a arises exclusively from the loss in FLD efficiency with larger fiber volume fraction. This is proved in Fig. 6 for HIPS/GF composites, where η^b_{FLD} for independent IFSS estimations (around 14.7 MPa) at each fiber content are well-represented by Eq. 2's model curve, implementing the linear K–V_f dependence and constant IFSS.

In addition to V_f, FLD efficiencies can be continuously investigated as a function of applied strain as illustrated in

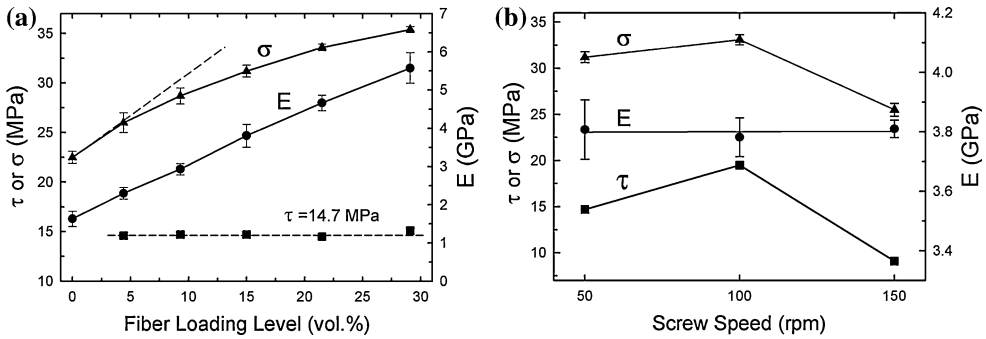

Fig. 3 Variation of tensile strength (σ), IFSS (τ), and Young's modulus (E) of HIPS/GF composites with **a** fiber volume fraction and **b** screw speed in extrusion

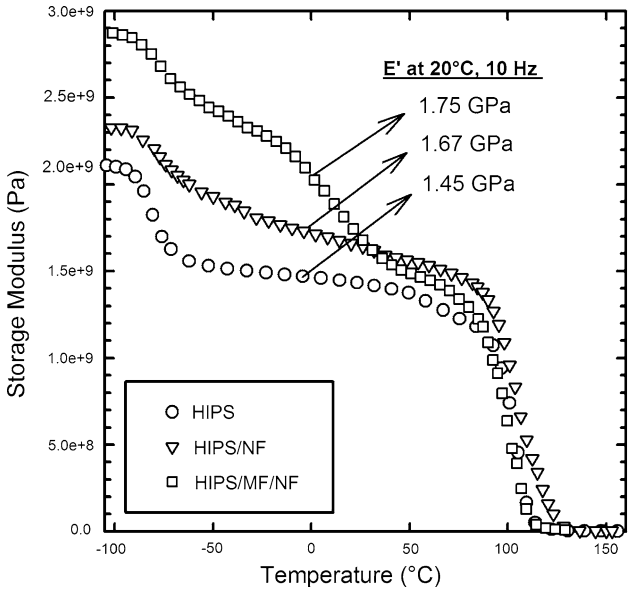

Fig. 4 DMA curves of HIPS, HIPS/MF, and HIPS/MF/NF as the fiber free matrices of short glass fiber reinforced composites

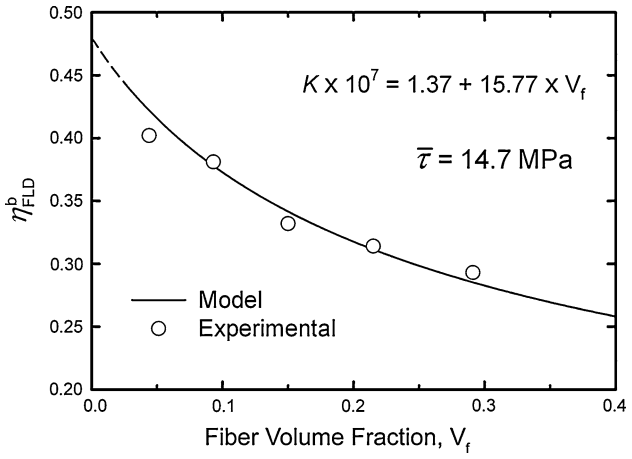

Fig. 6 Comparison of fiber content dependencies of experimental fiber length efficiency factors to the corresponding theoretically derived curve by the applied micromechanical model

Fig. 7a. These were plotted according to Eq. 2 by considering the τ and K values for each composite. Each curve starts from unity meaning that all fibers are longer than $\ell_c \approx 0$ for an initial infinitesimal strain. As strain develops, ℓ_c increases linearly according to $\ell_c = E_f \varepsilon d(2\tau)^{-1}$, and η_{FLD} decreases in the nonlinear form dictated by Eq. 2. It can be inferred from Fig. 7b that the experimental σ–ε responses of composites were well-reproduced by the micromechanics approach with determined τ, K and η_{FOD} values. The nonlinear nature of these σ–ε curves originates from the combination of loss in fiber length efficiency with strain in Fig. 7a and nonlinear contribution of the thermoplastic matrix itself. Since the utilized micromechanics approach is capable of reproducing the experimental mechanical behavior well (Fig. 7b), when combined with a predetermined K–V_f relation, composite stress at a given strain can be safely predicted for any hypothetical fiber loading lying in the range between the experimentally studied values. However, the calculation of stress at a given strain does not provide information on strength or failure.

By investigating HIPS/GF composites, properties of the matrix (such as morphology, thermal expansion, mechanical behavior, etc.) were held almost fixed. This allowed trends observed in apparent IFSS to be directly attributed to micromechanical parameters and IFSS turned out to be independent of V_f. In the following paragraphs, however, the effects of alteration in properties of the "matrix" with micro- and/or nano-filler modification on the fiber/matrix IFSS will be discussed.

Besides the main fiber–fiber attrition, introduction of fillers with different length-scales into the extruder results in fiber–filler attritions and increased melt viscosity during extrusion. These can easily induce larger K values as shown in Fig. 8a. Although MF loading is much larger than that of NF, the latter induced nearly the same degradation in fiber lengths relative to the reference HIPS/GF. This may be due to the higher potential of NF to influence melt viscosity and more severe attrition effect of finely dispersed NF on fiber surfaces during processing. Introduction of MF and NF together led to a cumulative effect and caused further shifting of the FLD to shorter lengths.

Figure 9 compares the stress–strain behavior of various fiber free matrices and corresponding short-fiber

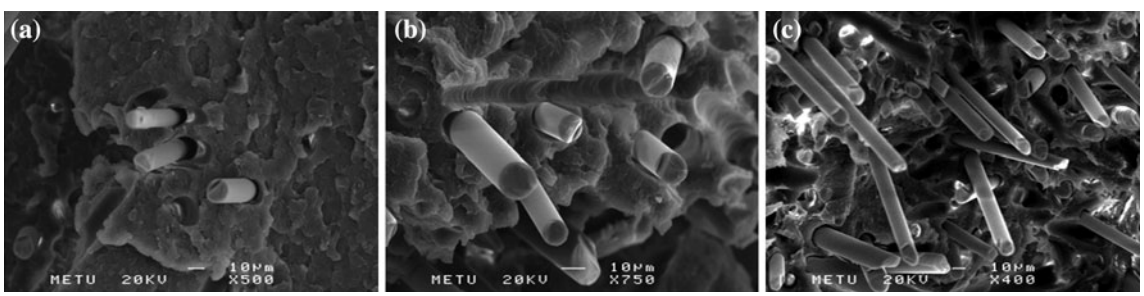

Fig. 5 SEM images of fracture surfaces of HIPS/GF composites with short glass fiber contents of **a** 10 wt%, **b** 30 wt%, and **c** 50 wt%

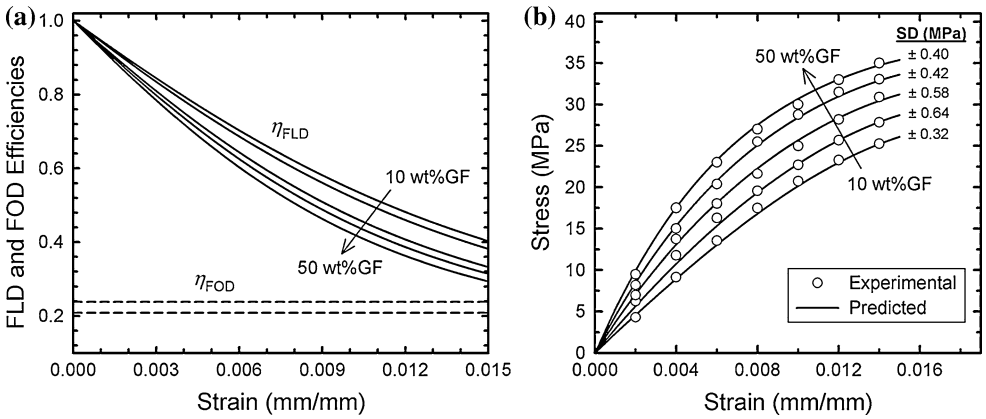

Fig. 7 **a** Fiber length and orientation efficiencies plotted as a function of strain for HIPS/GF composites where η_{FOD} values remain between the horizontal dashed lines in an interval of 0.21–0.24, **b** comparison of experimental and predicted stress–strain curves of HIPS/GF composites where the standard deviation (SD) of residuals for the prediction range from 0.32 to 0.58 MPa

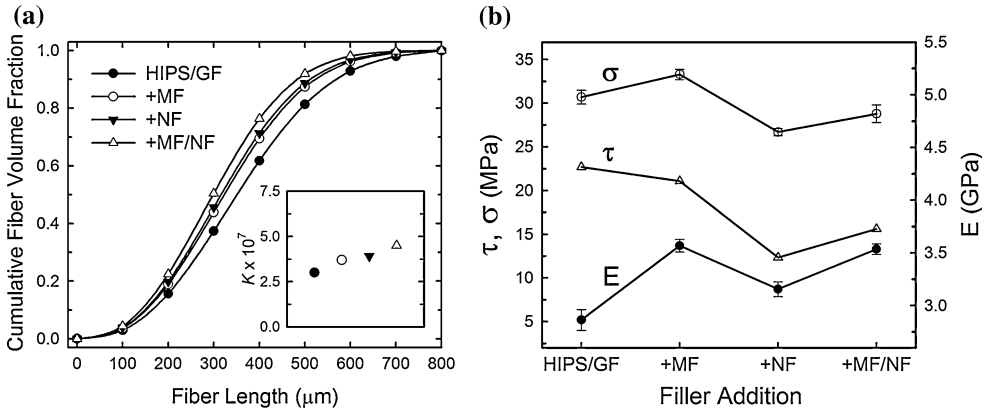

Fig. 8 Variations of **a** FLD, and, **b** tensile strength (σ), IFSS (τ), and Young's modulus (E) of filler modified HIPS/GF composites. *Inset* in **a** shows the variation of residual fiber lengths represented by K values of FLDs

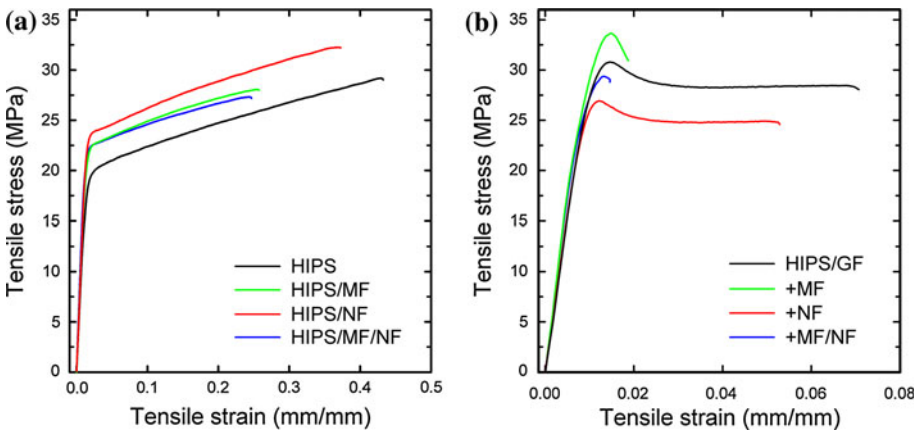

Fig. 9 Stress–strain curves showing the influence of fillers with different length-scales on the behavior of **a** neat HIPS and **b** HIPS/GF

composites. Incorporation of NF into the neat matrix at a low loading level resulted in significantly increased yield strength and tensile strength with only slight reduction in elongation at break. Although MF addition promoted some strengthening with respect to the neat matrix, ductility was adversely affected due to higher loading level and larger particle size of the filler. Dominated by MF with a high loading level in the matrix, the fiber free matrix containing both fillers showed a stress–strain behavior similar to MF containing sample. The influence of micro- and nano-fillers on the tensile behavior of fiber-reinforced composites followed different trends due to the changes in residual fiber lengths and strength of the fiber/matrix interface caused by the presence of fillers with different length-scales.

Although MF resulted in fiber breakage to nearly the same extent as NF, it had no significant effect on IFSS (Fig. 8b). Accordingly, tensile strength of +MF hybrid composite slightly increased due to the gain in stiffness relative to HIPS/GF. However, NF modification reduced the IFSS and composite strength. The recovery of composite modulus and the slight increase in IFSS in +MF/NF addition with respect to +NF compensated the extensive K increase and yielded a slight recovery of composite strength. The probability of micron-sized particles to locate

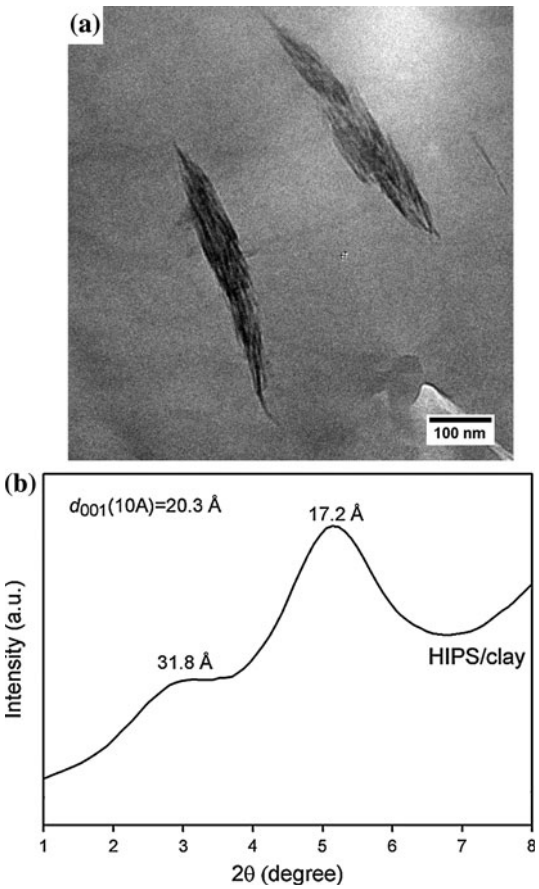

Fig. 10 **a** TEM image and **b** XRD pattern of HIPS/NF sample containing montmorillonite crystallites exhibiting partial polymer intercalation as inferred from the low angle reflection corresponding to an increased *d*-spacing from 20.3 to 31.8 Å

in the vicinity of a fiber/matrix interface is relatively low due to large expected filler-fiber spacings. However, in the case of NF, due to dispersion of clay aggregates into finer crystallites upon melt-processing as shown by the TEM image in Fig. 10, the effect of NF on fiber/matrix interfacial zone is expected to be more pronounced than that of MF.

Considering DMA curves provided in Fig. 4, it is clear that NF promotes significant stiffening below the glass transition of PS phase compared to neat HIPS. Storage modulus (E') measured at 20 °C was increased from 1.45 to 1.67 GPa with NF addition at a very low loading level (3 wt%). Contrarily, a slight increase from 1.67 to 1.75 GPa was seen with MF addition despite its relatively large loading level (15 wt%). Since NF is able to be located in the vicinity of fiber/matrix interfaces as well as in the bulk of the matrix, it can be postulated that considerable alteration of polymer matrix properties at the interfacial zone are expected which might be the cause of decreased IFSS. One explanation could be the thermal contraction of polymer chains in close vicinity of fiber/matrix interface being restricted in the presence of NF as a result of decreased thermal expansion coefficient. The presence of finely dispersed nano-fillers with large aspect ratio, high modulus, and low thermal expansion coefficient was shown to significantly decrease the linear thermal expansion coefficient of thermoplastic polymer matrices even at very low loading levels [38–41]. This would greatly reduce the thermal residual stresses developing during post-processing due to thermal expansion coefficient mismatch between ceramic fibers and polymer matrix and could directly show up as lowered apparent IFSS.

Thus, reduced tensile strength in the presence of NF is due to the combination of effects of NF on fiber lengths, IFSS and especially the physical properties of polymer matrix. Comparing Fig. 11a, b, it is seen that there exists no significant influence of MF on matrix morphology in fracture surface. Unlike MF, due to the fine dispersion of NF, matrix morphology was clearly altered both within the bulk and in the vicinity of fibers. To sum up, reduced tensile strength in the presence of NF is due to the combination of effects of NF on fiber lengths, IFSS and especially the physical properties of polymer matrix.

Conclusion

Interfacial shear strength in short-glass fiber-reinforced composites was determined by a micromechanical approach to understand the influence of fiber content, processing condition, and presence of micro- and nano-scale fillers on the fiber/matrix interface in a model system based on HIPS/GF. In order to estimate the apparent IFSS, the approach requires experimental tensile test data and residual fiber length distributions as input.

The extent of fiber length degradation was found to progressively increase with fiber volume fraction due to higher probability of attrition contacts during processing. IFSS was shown to be close to the shear yield strength of HIPS and independent of fiber content in HIPS/GF system, where matrix morphology is not altered by varying the fiber content and thermal residual stresses can relax readily upon processing. The decreasing composite strengthening rate with fiber loading was attributed to the nonlinear loss in utilized fiber length distribution efficiency function. Furthermore, the nonlinearity of stress–strain curves was shown to be related to the characteristic decrease of fiber length efficiency with strain and the nonlinear contribution from the polymer matrix itself. Utilizing these in the current micromechanics framework, experimental stress–strain behaviors of HIPS/GF composites were successfully reproduced with determined micromechanical parameters.

Despite the very low loading level, nano-filler modification shortened reinforcing fibers as much as the

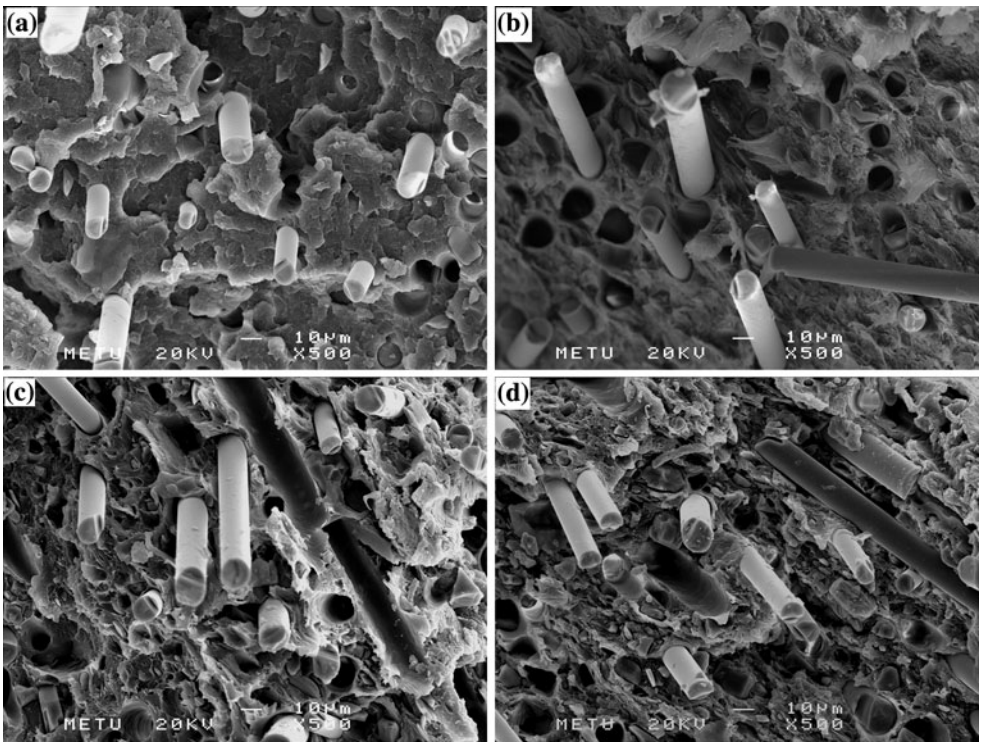

Fig. 11 SEM images of fracture surfaces of **a** HIPS/GF, **b** +MF, **c** +NF and +MF/NF composites, showing the correlation of predicted IFSS values and morphology of interfacial zones in fracture surfaces

micro-filler due to the fine dispersion in the matrix. While micro-filler was found to have no significant effect on interfacial strength, nano-filler modification reduced the IFSS, which was explained by the limited post-processing thermal contraction of the polymer matrix due to fine dispersion of rigid, high-aspect ratio nanoparticles both within bulk of the matrix and near fiber/matrix interfaces.

References

1. Desaeger M, Verpoest I (1993) Compos Sci Technol 48:215
2. Marotzke C (1993) Compos Interf 1:153
3. Piggott MR (1991) Compos Sci Technol 42:57
4. Piggott MR (1997) Compos Sci Technol 57:965
5. Piggott MR, Dai SR (1991) Polym Eng Sci 31:1246
6. Piggott MR, Reboredo MM (1995) Compos Interf 2:457
7. Pisanova E, Zhandarov S, Mader E, Ahmad I, Young RJ (2001) Compos Pt A-Appl Sci Manuf 32:435
8. Thomason JL (2001) Compos Sci Technol 61:2007
9. Thomason JL (2002) Compos Pt A-Appl Sci Manuf 33:331
10. Thomason JL (2002) Compos Sci Technol 62:1455
11. Thomason JL (2002) Compos Pt A-Appl Sci Manuf 33:1283
12. Isitman NA, Aykol M (2010) Compos Interfaces 17:49
13. Gunduz HO, Isitman NA, Aykol M, Kaynak C (2009) Polym-Plast Technol Eng 48:1046
14. Isitman NA, Aykol M, Kaynak C (2010) Compos Struct 92:2181
15. Isitman NA, Aykol M, Ozkoc G, Bayram G, Kaynak C (2010) Polym Compos 31:392
16. Thomason JL (2006) Polym Compos 27:552
17. Thomason JL (2007) Compos Pt A-Appl Sci Manuf 38:210
18. Thomason JL (2008) Compos Pt A-Appl Sci Manuf 39:1618
19. Zhao CS, Huang FL, Xiong WC, Wang YZ (2008) Polym Degrad Stab 93:1188
20. Isitman NA, Gunduz HO, Kaynak C (2010) J Fire Sci 28:87
21. Kaynak C, Gunduz HO, Isitman NA (2010) J Nanosci Nanotechnol 10:7374
22. Yoo Y, Spencer MW, Paul DR (2011) Polymer 52:180
23. Vlasveld DPN, Parlevliet PP, Bersee HEN, Picken SJ (2005) Compos Pt A-Appl Sci Manuf 36:1
24. Ramani K, Bank D, Kraemer N (1995) Polym Compos 16:258
25. Vonturkovich R, Erwin L (1988) Polym Eng Sci 23:743
26. Wolf HJ (1994) Polym Compos 15:375
27. Aykol M, Isitman NA, Firlar E, Kaynak C (2008) Polym Compos 29:644
28. Bader MG, Bowyer WH (1972) J Phys D-Appl Phys 5:2215
29. Bowyer WH, Bader MG (1972) J Mater Sci 7:1315. doi: 10.1007/BF00550698
30. Fu SY, Yue CY, Hu X, Mai YW (2001) J Mater Sci 20:31. doi: 10.1023/A:1006750328386
31. Chin WK, Liu HT, Lee YD (1988) Polym Compos 9:27
32. Fu SY, Mai YW, Ching ECY, Li RKY (2002) Compos Pt A-Appl Sci Manuf 33:1549
33. Ulrych F, Sova M, Vokrouhlecky J, Turcic B (1993) Polym Compos 14:229
34. Fu SY, Lauke B, Li RKY, Mai YW (2006) Compos Pt B-Eng 37:182
35. Ozkoc G, Bayram G, Bayramli E (2005) Polym Compos 26:745
36. Fu SY, Lauke B (1998) Compos Pt A-Appl Sci Manuf 29:631

37. Curtis PT, Bader MG, Bailey JE (1978) J Mater Sci 13:377. doi: 10.1007/BF00647783
38. Uddin F (2008) Metall Mater Trans A 39:2804
39. Yoon PJ, Fornes TD, Paul DR (2002) Polymer 43:6727
40. Kim DH, Fasulo PD, Rodgers WR, Paul DR (2008) Polymer 49:2492
41. Utracki LA (2009) Eur Polym J 45:1891